Letter

Real modes and null memory contributions in effective-one-body models

Simone Albanesi*

Theoretisch-Physikalisches Institut, Friedrich-Schiller-Universität Jena, 07743, Jena, Germany and INFN sezione di Torino, Torino, 10125, Italy

(Received 12 November 2024; revised 13 April 2025; accepted 6 May 2025; published 9 June 2025)

We introduce a novel approach to describe real-valued $m = 0$ modes from inspiral to merger and ringdown in effective-one-body models, including both oscillatory and null memory contributions. A crucial aspect of the modelization of the oscillatory part is the complexification of the real modes via a Hilbert transform. This procedure allows for an accurate description of the merger-ringdown waveform by applying standard approaches employed for the complex $m > 0$ modes, which include source-driven effects. The physical signal is then recovered by solely considering the real part. We apply this method in the extreme-mass-ratio regime, considering particle-driven linear gravitational perturbations in Schwarzschild and Kerr spacetimes. We then extend our description to spin-aligned, quasicircular, comparable-mass binaries providing hierarchical fits incorporating the test-mass limit. The postmerger waveform is then matched with an inspiral effective-one-body waveform. By adopting `TEOBResumSGIOTTO` as our baseline, we also include the displacement memory in the (2, 0) mode through Bondi–van der Burg–Metzner-Sachs balance laws, thus providing a complete effective-one-body model incorporating both oscillatory and null memory effects. The accuracy of this model is validated against the hybrid numerical relativity surrogate `NRHybSur3dq8_CCE`, finding, for the quadrupole of the equal mass nonspinning case, a LIGO noise-weighted mismatch of $\bar{\mathcal{F}} = 6 \times 10^{-4}$ at $50M_\odot$ for the inclination that maximizes the contribution of the (2, 0) mode.

DOI: 10.1103/PhysRevD.111.L121501

Introduction. With the detections from the LIGO-Virgo-KAGRA (LVK) network [1,2], gravitational wave (GW) astronomy has now become a standard tool for exploring the Universe [3–5]. Waveform models for compact binaries are central to this field, both for detection and data analysis, making it essential to provide accurate GW models. Moreover, the advent of next-generation detectors, such as Einstein Telescope [6,7], LISA [8], and Cosmic Explorer [9], requires even further advancements in waveform modeling, not only in accuracy [10], but also in capturing all the physically relevant phenomena [11]. The effective-one-body (EOB) approach [12–14] is capable to accurately model GWs from compact binaries, once calibrated and complemented with numerical relativity (NR) data [15–17]. This approach does not only describe standard quasicircular binary black holes (BBHs) [18,19] but can be also employed to model binaries in presence of matter [20–23], eccentricity [24–32], and spin-precession [33–38], eventually jointly [39–42]. However, state-of-the-art EOB models do not include $m = 0$ modes in the coprecessing frame, despite them being particularly relevant when the radial acceleration is large, *e.g.*, on eccentric orbits or during the plunge. In this work, we devise a strategy to incorporate their description, from inspiral to merger and ringdown, considering both oscillatory contributions and displacement memory effects. To build our model for the oscillatory part, we consider numerical results obtained by solving linear perturbations sourced by test-particle dynamics [43–47] with `RWZHyp` [48–50] and `Teukode` [51], together with waveforms obtained from the surrogate model `NRHybSur3dq8` [52], which is built using NR simulations of the SXS Collaboration [53–66]. After having discussed some phenomenological aspects, we start by extending the postmerger model of Ref. [67] to the real $m = 0$ oscillatory modes through a complexification achieved with a Hilbert transform [68,69]. We then provide a closed-form representation of the oscillatory postmerger for the (2, 0) mode across the parameter space of spin-aligned binaries with generic mass ratios by means of hierarchical fits. This postmerger model is then matched with an inspiral EOB waveform based on Ref. [24], using standard next-to-quasicircular (NQC) corrections [16].

The (2, 0) mode is also sourced by the outgoing gravitational radiation, thus manifesting a nonlinear memory

*Contact author: simone.albanesi@uni-jena.de

Published by the American Physical Society under the terms of the Creative Commons Attribution 4.0 International license. Further distribution of this work must maintain attribution to the author(s) and the published article's title, journal citation, and DOI.

contribution [70–73]. This effect, which is inherently related to the radiated energy flux [71], has been studied for quasicircular binaries in post-Newtonian (PN) theory [74,75] and in minimal-waveform models, where an EOB inspiral/plunge waveform is completed with a postmerger model purely based on a quasi-normal-mode (QNM) description [76,77]. Null memory contributions for eccentric inspirals have also been studied within the PN framework [78,79] and the EOB one [80]. These effects have been resolved in NR simulations only recently [81,82], by using Cauchy characteristic extraction (CCE) [83–87]. It should be noted that the strain, and memory effects in particular, are inherently linked to the Bondi–van der Burg–Metzner-Sachs (BMS) group [88,89], which is the symmetry group of asymptotically flat spacetimes at future null infinity (Poincaré group plus supertranslations). Therefore, using BMS balance laws, null memory effects can also be added in postprocessing to NR simulations [90,91]. The displacement memory in the (2, 0) mode has been also included in some inspiral-merger-ringdown (IMR) waveforms models [76,77,92], and in particular, in `IMRPhenomTHM` [93]. Memory effects have been searched in LVK data [94,95] and are potentially detectable with future observations [96–100].

We then apply our strategy employing `TEOBResumS-GIOTTO` [18] as a baseline, thus completing this model by including the description of the (2, 0) multipole for spin-aligned quasicircular BBHs with generic mass ratio. The oscillatory part is described with an EOB waveform completed with the aforementioned Hilbert postmerger model, while the null memory contribution is computed from BMS balance laws and matched, at low-frequencies, with the PN result [78,79,92]. The model is validated against the hybrid NR-surrogate `NRHybSur3dq8_CCE` [101], whose waveforms are in the same BMS frame as the EOB ones, thus avoiding any coordinate ambiguity [66,102]. A comparison for the quadrupolar strain with this surrogate and a NR SXS simulation [66] is anticipated in Fig. 1. More details are discussed in the Conclusions.

Conventions. We use geometric units $G = c = 1$. The GW strain is decomposed in multipoles on spin-weighted spherical harmonics as $h_+ - ih_\times = \sum_{\ell m} {}_{-2}Y_{\ell m}(\Theta,\Phi) R^{-1} h_{\ell m}$, being R the distance of the observer. Multipoles are further decomposed in amplitude and phase as $h_{\ell m} = A_{\ell m} e^{-i\phi_{\ell m}}$. The waveform frequency is computed as $\omega_{\ell m} = \dot{\phi}_{\ell m}$, where the dot indicates a time derivative. If not specified otherwise, length scales are normalized with the total rest mass of the system $M = m_1 + m_2$, where $m_{1,2}$ are the masses of the two black holes ($m_1 > m_2$). The symmetric mass ratio is defined as $\nu = q/(1+q)^2$, where $q = m_1/m_2$. The dimensionless Kerr spin is denoted as $\hat{a}$, with $\hat{a} \geq 0$ ($\hat{a} < 0$) for prograde (retrograde) equatorial orbits. For comparable-mass binaries, the dimensionless black hole spins are instead denoted as $\chi_{1,2}$. The time corresponding to the peak of the (2, 2) amplitude is indicated as $t^{\rm peak}_{A_{22}}$.

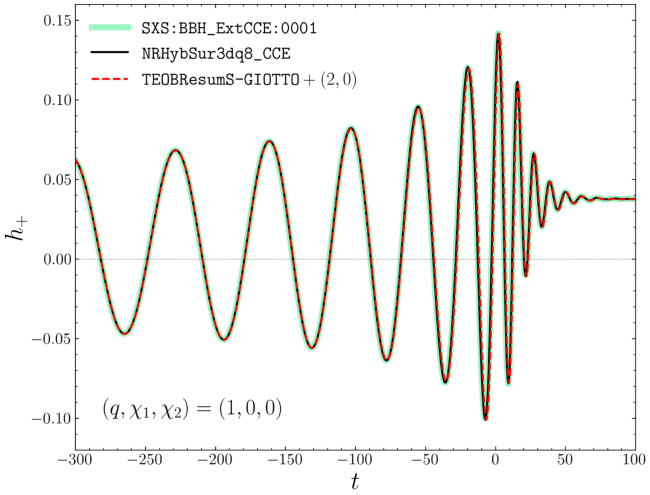


FIG. 1. Quadrupolar strains for the equal mass nonspinning case and observational direction $(\Theta, \Phi) = (\frac{\pi}{2}, 0)$. We consider the simulation `SXS:BBH_ExtCCE:0001` [66] (thick green), the surrogate `NRHybSur3dq8_CCE` [101] (solid black), and the EOB model `TEOBResumS-GIOTTO` [18] completed with the (2, 0) mode as discussed in this work (dashed red).

EOB dynamics and test-mass limit. The standard EOB approach consists in mapping the 2-body PN dynamics to the motion of a particle in an effective metric, which is a ν deformation of the Schwarzschild or Kerr one [12–14]. The EOB Hamiltonian, together with a PN-resummed prescription for the radiation reaction, provides Hamilton's equations that can be solved to obtain the effective dynamics, from which is then possible to analytically compute the multipolar waveform at infinity. By setting to zero the ν corrections in the conservative sector and keeping leading-order contribution in the radiation reaction, we can evolve inspirals in Schwarzschild and Kerr spacetimes, thus obtaining a first-order description of extreme-mass ratio binaries. However, note that higher-order corrections in the mass ratio are needed to describe real astrophysical scenarios [103]. Given test-mass dynamics, we can numerically compute the linear-order gravitational perturbations sourced by the motion of the particle. This approach has been extensively used to gain insights into prescriptions to use for binaries with generic mass-ratio [16,104–106]. In this work, we start by considering the quasicircular inspiral of Ref. [106], obtained by solving the Regge-Wheeler and Zerilli equations with a test-particle source term [43–46] using the time-domain code `RWZHyp` [48–50]. We then explore the Kerr case, by solving the Teukolsky equation [47] for 11 quasicircular configurations `Teukode` with [51]. The test-mass simulations are listed in Table S2 of the Supplemental Material (SM) [107].

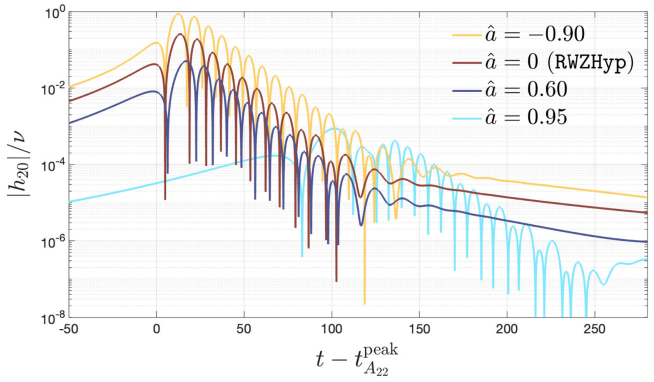


FIG. 2. (2, 0) modes generated by quasicircular evolutions in Schwarzschild and Kerr for different spin parameters $\hat{a}$. Aligned with respect to $t^{\rm peak}_{A_{22}}$.

Phenomenology. In the test-mass limit, the relevance of the (2, 0) mode changes substantially with the dimensionless Kerr spin $\hat{a}$, as shown in Fig. 2. Indeed, the (2, 0) mode is enhanced for $\hat{a} < 0$, while it is suppressed for high positive spins. This can be understood by noting that the $m = 0$ multipoles are radial modes, and that the last stable orbit is larger for retrograde than for prograde orbits [120], thus leading to a more radial plunge. Moreover, the peak of the signal is strongly delayed with respect to $t^{\rm peak}_{A_{22}}$, as shown by the $\hat{a} = 0.95$ case. We also observe that the tail [121–123] of the $m = 0$ modes is more relevant than for $m > 0$ ones, as expected.[1] Indeed, in Schwarzschild the transition from QNM to tail for the dominant mode occurs at $t \sim t^{\rm peak}_{A_{22}} + 230$, when $A_{22}/\nu \sim 5 \times 10^{-9}$, while for the (2, 0) mode it occurs at $t \sim t^{\rm peak}_{A_{22}} + 120$, when $A_{20}/\nu \sim 5 \times 10^{-5}$. For the RWZHyp simulation here considered, we find that the tail is well described by a power law $h^{\rm tail}_{20} \propto (t - t^{\rm peak}_{A_{22}})^{-2.787}$ (see inset of Fig. 3). However, in general, the tail can have rather complicated behaviors, as extensively discussed in Ref. [124]. Eccentric RWZHyp simulations show that the tail enhancement due to the orbital eccentricity observed for the $m > 0$ modes [106,124,127,128] occurs also for the (2, 0) mode in Schwarzschild.

By inspecting the SXS catalog [65], we observe an enhancement of the (2, 0) oscillatory mode for binaries with antialigned spins also in the comparable-mass case. However, as the symmetric mass ratio increases, the null memory contribution gains importance, as it is linked to the radiated energy flux. For the same reason, the memory contribution is enhanced for spin-aligned binaries, where, instead, the oscillatory part is suppressed. The accurate modeling of both contributions is thus needed.

[1]Indeed, the tail is enhanced by radial motion; see, *e.g.*, Ref. [124] and Eq. (22) therein or Refs. [125,126].

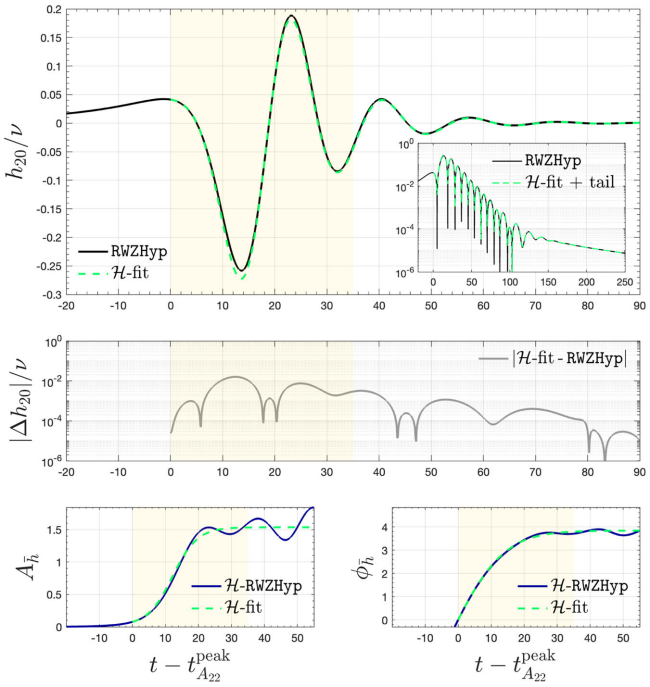


FIG. 3. Upper panel: (2, 0) mode for the Schwarzschild configuration. We show the numerical waveform (black) and the Hilbert fit (dashed green). Middle panel: corresponding residual. Bottom panels: QNM-rescaled amplitudes and phase of the complexified numerical (2, 0) mode (blue) and corresponding Hilbert fits (dashed green). The vertical bands mark the $\mathcal{H}$-fitting interval.

Hilbert postmerger model. IMR models have to be completed with analytical ringdown models built employing NR simulations [15,16,67,129]. In particular, Ref. [67] proposed to factorize the fundamental QNM from the numerical multipoles, thus obtaining a QNM-rescaled mode. The latter is defined as $\bar{h}(\tau) \equiv e^{\sigma_1 \tau + i\phi_0} h(\tau)$, where $\sigma_1 = \alpha_1 + i\omega_1$ is the fundamental QNM, ϕ_0 is the phase at the starting time of the fit $t^0_{\rm fit}$, $\tau = (t - t^0_{\rm fit})/M_f$, and M_f is the mass of the remnant. This signal thus still contains all the source-driven transient contributions, higher QNM overtones, and eventual non-linearities that are in numerical waveforms. The closed-form description is then achieved by fitting the amplitude and the phase of the rescaled waveform, $\bar{h} = A_{\bar{h}} e^{i\phi_{\bar{h}}}$. The model's accuracy relies in the simple shape of the amplitude and phase of $\bar{h}$, which can be easily fitted with activationlike monotonic functions.

While this approach has been successfully adopted for complex modes, it cannot be readily applied to the real $m = 0$ modes due to its inherently complex nature. Moreover, complex signals allows us to impose continuity conditions on amplitude and frequency, which is important for constraining fit parameters and for applying NQC corrections, as we will discuss in the next section. We thus propose to (i) complexify the $m = 0$ modes, (ii) apply

a model similar to the one discussed above, (iii) get the physical signal by solely considering the real part.

To this end, we use the Hilbert transform [68,69] of a function $v(t)$, defined as $\mathcal{H}[v](t) \equiv 2/\pi \lim_{\epsilon\to 0} \int_\epsilon^\infty \frac{v(t-\tau)-v(t+\tau)}{2\tau} d\tau$. Its meaning is clarified by the relation with the Fourier transform $\mathcal{F}[v](\omega)$,

$$\mathcal{F}[\mathcal{H}[v]](\omega) = -i\mathrm{sgn}(\omega)\mathcal{F}[v](\omega), \tag{1}$$

where $\mathrm{sgn}(x)$ is the sign function. Therefore, the Hilbert transform shifts the negative (positive) frequencies of $v(t)$ by $\frac{\pi}{2}$ $(-\frac{\pi}{2})$. Given a real signal $v_{\rm R}(t)$, the Hilbert transform can be used to create an analytical signal $v_{\mathcal{H}}(t) = v_{\rm R}(t) - i\mathcal{H}[v](t)$. If we apply this complexification to the $m = 0$ modes, we find amplitudes and phases that *look like* the ones of the $m > 0$ modes. We can thus generalize the phenomenological ringdown model of Ref. [67] to real modes by simply working with their complexifications.

The Hilbert transform has to be performed only when building the model; once the parameters of the *Ansätze* have been found, we can just evaluate the closed-form postmerger waveform.

We start by applying this procedure to the (2, 0) mode of the Schwarzschild case. It is known that for complex higher modes that are strongly delayed with respect to the (2, 2) one, it is convenient to apply the model of Ref. [67] from $t^{\rm peak}_{A_{22}}$ rather than from $t^{\rm peak}_{A_{\ell m}}$ [130]. We thus perform our Hilbert fit starting from $t^0_{\rm fit} = t^{\rm peak}_{A_{22}}$. This choice facilitates the matching with the inspiral waveform discussed in the next section. The amplitude and phase of the complexified QNM-rescaled waveforms are modeled with *Ansätze* similar to the ones proposed in Ref. [67], as detailed in the SM [107]. Note that some coefficients are constrained in terms of numerical quantities, $\{A_0, \dot{A}_0, \omega_0\}$, by imposing continuity conditions. The results for the Schwarzschild case are displayed in Fig. 3. In the bottom panels, we report the amplitude and phase of the complexified numerical waveform (dark blue), together with the primary Hilbert fits (dashed green). The chosen *Ansätze* are able to catch the behavior of the complexified signal, yielding a real (2, 0) mode (top panel) with analytical/numerical residual $\lesssim 0.02$ (middle panel). However, it should be noted that the phase template is more accurate than the amplitude one, meaning that future works could explore different choices for the amplitude *Ansatz* to further improve the accuracy of this procedure. Moreover, the oscillations in the complexified signal observed for $t \gtrsim t^{\rm peak}_{A_{22}} + 20$ are likely to be, at least in part, an artefact of the transform. Indeed, they also appear when complexifying the real part of the (2, 2) mode, while they are less evident in the corresponding physical waveform.

The postmerger Hilbert fit can readily be applied to higher modes, Kerr configurations, and NR simulations. While some primary fits performed over SXS simulations are shown in the SM [107], we build our model for the oscillatory contribution using waveforms generated with `NRHybSur3dq8` [52]. Once the coefficients have been found for enough configurations, we can fit them over the parameter space. For the mass and spin of the remnant, we use the fits of Refs. [131,132], while for the coefficients of the new model and $\{A_0, \dot{A}_0, \omega_0\}$, we perform a hierarchical fit. We first perform quadratic fits of test-mass and nonspinning configurations, separately. We then complete our model by merging these two results over the parameter space identified by $(\nu, \tilde{a}_0)$, where $\tilde{a}_0 = (m_1\chi_1 + m_2\chi_2)/M$ generalizes the Kerr spin. The explicit *Ansätze* and the coefficients found are given in the SM [107].

Matching with inspiral waveform. A formally Newtonian expression for the inspiral $m = 0$ modes can be obtained following Ref. [24]. For the (2, 0) mode, this reads

$$h^{\rm inspl}_{20} = 4\sqrt{\frac{2\pi}{15}}\nu(r\ddot{r} + \dot{r}^2). \tag{2}$$

Note that 2.5PN corrections for $h^{\rm inspl}_{20}$ have been recently computed [80,133] and might be useful for generic orbits. However, since here we are focusing on the plunge of quasicircular evolutions, we do not consider them.[2] To match this waveform to the postmerger model previously discussed, we can also complexify $h^{\rm inspl}_{20}$ with a Hilbert transform. The matching can be then performed with standard EOB techniques, which involve NQC corrections. Note that for NQC corrections to work effectively, well-defined and preferably monotonic amplitude and phase are needed. We achieve these requirements through the aforementioned complexification. Although this matching is a standard procedure in EOB models, we briefly discuss it in the SM [107] for completeness, along with minor technical details.

Null memory effects. Null memory effects [70–73], which are particularly relevant for comparable mass binaries, can be computed using BMS balance laws [91]. These relations connect the strain to the Bondi aspects (*i.e.*, the oscillatory parts discussed so far) and the radiated fluxes. More specifically, the displacement memory in the (2, 0) mode arises from the supertranslation conservation law and is thus sourced by the radiated energy flux. It can be written in terms of the most relevant multipoles as [93]

$$\begin{aligned} h^{\rm memo}_{20}(t) = {} & \frac{1}{7}\sqrt{\frac{5}{6\pi}}\int_{t_0}^{t} |\dot{h}_{22}|^2 dt - \frac{1}{14}\sqrt{\frac{5}{6\pi}}\int_{t_0}^{t} |\dot{h}_{21}|^2 dt \\ & + \frac{5}{2\sqrt{42\pi}}\int_{t_0}^{t} \left(\dot{h}^{\rm Re}_{22}\dot{h}^{\rm Re}_{32} + \dot{h}^{\rm Im}_{22}\dot{h}^{\rm Im}_{32}\right) \\ & - \frac{2}{11}\sqrt{\frac{2}{15\pi}}\int_{t_0}^{t} |\dot{h}_{44}|^2 dt. \end{aligned} \tag{3}$$

[2]Moreover, PN results are known to be unreliable in the late stages of the evolution.

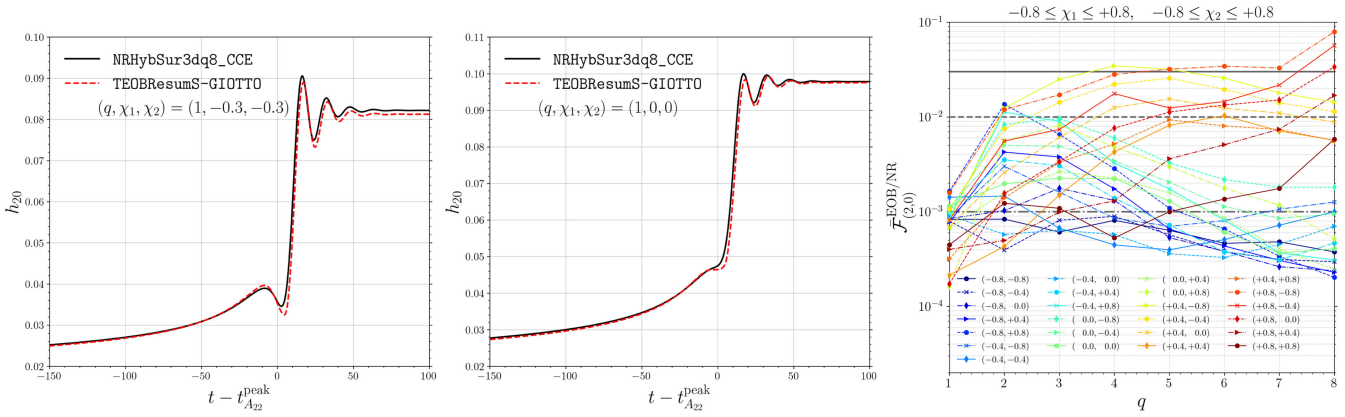


FIG. 4. Comparisons of (2, 0) modes given by `NRHybSur3dq8_CCE` and the ones computed in this work using `TEOBResumS-GIOTTO` as a baseline. Left and middle panels: time-domain comparisons. Right panel: LIGO-weighted mismatches of the (2, 0) modes for different mass ratios and spin configurations. The legend in the right panel reports (χ_1, χ_2).

Formally, one should consider $t_0 \to -\infty$, but in practical application t_0 is the starting time of the evolution. This means that, if we extrapolate back in time, we get the unphysical property $h^{\rm memo}_{20} \neq 0$ for $t \to -\infty$. This can easily fixed by matching this memory contribution to the PN formula [74,75], which correctly vanishes at zero frequency. Note that Ref. [93] followed a similar approach. Technical details on this matching are discussed in the SM [107]. Therefore, given the $m > 0$ EOB multipoles, we can compute the full (2, 0) mode as $h_{20} = h^{\rm osc}_{20} + h^{\rm memo}_{20}$, where $h^{\rm osc}_{20}$ is the oscillatory contribution previously discussed.

EOB/NR comparisons. We now apply the methodology here introduced to the EOB model `TEOBResumS-GIOTTO` [18] and compare it with NR results. To avoid ambiguities linked to different BMS frames, we consider the surrogate `NRHybSur3dq8_CCE` [101], whose waveforms are already in the PN frame, as the EOB ones. Time-domain comparisons for two meaningful equal mass cases are reported in Fig. 4, showing that our model is able to capture the main features of the numerical waveform. Since the ringdown modeling of the higher modes enter in the computation of the final EOB offset, improving their description would yield an offset closer to the numerical one. This is however beyond the scope of this work, and thus deferred to future investigations. Some additional time-domain comparisons are reported in the SM [107]. To assess the accuracy more systematically, we also consider frequency-domain mismatches for the (2, 0) mode for different mass ratios and spins in the right panel of Fig. 4. We consider the noise curve of Advance LIGO [134] and a reference mass of $50M_\odot$. More technical details are reported in the SM [107]. The model is generally accurate, especially for equal-mass binaries, where all the mismatches are below 2×10^{-3}, and for high mass-ratio cases with low spins. However, higher mismatches are obtained for configurations, where χ_1 and χ_2 strongly differ. This can be understood by considering that we reduce the dimensionality of the fits across the parameter space by employing the effective spin $\tilde{a}_0$ rather than the two individual spins $\chi_{1,2}$ separately.

We conclude by discussing the quadrupolar strains anticipated in Fig. 1, which are computed for an observer with line of sight that maximizes the contribution of the (2, 0) mode ($\Theta = \frac{\pi}{2}$). We compare our EOB model with the results from `NRHybSur3dq8_CCE` and the equal mass nonspinning simulation of the `ExtCCE` SXS catalog [66]. Note that the SXS waveform is not in the PN frame, but we can obtain a good agreement with the surrogate by (i) mapping it to the superrest frame with the package `SCRI` [135–138], (ii) shifting its (2, 0) mode in order to match the final offset of the surrogate model. A more accurate, though more complex, procedure would involve mapping the SXS waveform to the PN frame as detailed in Refs. [66,102]. We remark that no additional offset shifting is performed for the EOB and `NRHybSur3dq8_CCE` waveforms. The agreement between the three shows the goodness of `TEOBResumS-GIOTTO` completed with the (2, 0) mode as discussed in this work. The EOB/NR mismatch for the complete quadrupolar waveform in this case is $\bar{\mathcal{F}} = 6 \times 10^{-4}$.

Conclusions. We have proposed a method to include the description of the real $m = 0$ modes in the EOB framework, thus completing the multipolar structure of IMR EOB waveforms for spin-aligned quasicircular BBHs. In particular, we have discussed how to model the oscillatory postmerger of such modes by first complexifying them with a Hilbert transform and then using a postmerger *Ansatz* based on Ref. [67], as typically done for $m > 0$ modes. We thus effectively include source-driven and higher QNM overtones contributions. This model has been applied to a set of test-mass simulations, hence showing its applicability in the linear perturbation regime. We then focused on the

(2, 0) modes and discussed how to employ NQC corrections to match the Hilbert postmerger model to the inspiral EOB waveform obtained with the approach introduced in Ref. [24]. The close-form description of the (2, 0) postmerger for the comparable mass case has been achieved by performing hierarchical fits for different mass ratios and effective spins using waveforms from `NRHybSur3dq8` [52]. These fits correctly include the test-mass limit. We have then discussed how to include null memory effects in EOB models, thus providing a complete description of the (2, 0) mode. Following this prescription, we have complemented `TEOBResumS-GIOTTO` and tested its validity against the surrogate `NRHybSur3dq8_CCE` [101]. We also performed a comparison with the equal mass nonspinning configuration of the SXS catalog of Ref. [66], showing a remarkable agreement.

Future works will focus on refining the methodology here introduced and on employing it to complete EOB models where the relevance of the (2, 0) mode is even more enhanced than for spin-aligned quasicircular binaries, such as precessing and eccentric models [42].

Acknowledgments. S. A. is grateful to R. Gamba, S. Bernuzzi, and A. Nagar for useful discussions through the whole development of this work. S. A. also thanks G. Carullo and M. De Amicis for useful comments and suggestions on the draft. S. A. acknowledges support from the Deutsche Forschungsgemeinschaft (DFG) project "GROOVHY" (BE 6301/5-1 Project No. 523180871). The EOB model `TEOBResumS-GIOTTO` and its version for generic orbital motion, `TEOBResumS-Dalí`, are publicly available at [139]. However, the procedure for computing the (2, 0) mode described in this work has not yet been implemented in the public code. In Fig. 2, we used a scientific color map provided by Ref. [140].

Data availability. The data supporting this study's findings are available within the article.

[1] J. Aasi *et al.* (LIGO Scientific Collaboration), Classical Quantum Gravity **32**, 074001 (2015).
[2] F. Acernese *et al.* (VIRGO Collaboration), Classical Quantum Gravity **32**, 024001 (2015).
[3] B. P. Abbott *et al.* (LIGO Scientific and Virgo Collaborations), Phys. Rev. X **9**, 031040 (2019).
[4] R. Abbott *et al.* (LIGO Scientific and Virgo Collaborations), Phys. Rev. X **11**, 021053 (2021).
[5] R. Abbott *et al.* (LIGO Scientific, VIRGO, and KAGRA Collaborations), Phys. Rev. X **13**, 041039 (2023).
[6] M. Punturo, M. Abernathy, F. Acernese, B. Allen, N. Andersson *et al.*, Classical Quantum Gravity **27**, 194002 (2010).
[7] M. Maggiore *et al.*, J. Cosmol. Astropart. Phys. 03 (2020) 050.
[8] P. Amaro-Seoane *et al.* (LISA Collaboration), arXiv:1702.00786.
[9] D. Reitze *et al.*, Bull. Am. Astron. Soc. **51**, 035 (2019).
[10] M. Pürrer and C.-J. Haster, Phys. Rev. Res. **2**, 023151 (2020).
[11] A. Gupta *et al.*, arXiv:2405.02197.
[12] A. Buonanno and T. Damour, Phys. Rev. D **59**, 084006 (1999).
[13] A. Buonanno and T. Damour, Phys. Rev. D **62**, 064015 (2000).
[14] T. Damour, Phys. Rev. D **64**, 124013 (2001).
[15] A. Buonanno, G. B. Cook, and F. Pretorius, Phys. Rev. D **75**, 124018 (2007).
[16] T. Damour and A. Nagar, Phys. Rev. D **76**, 064028 (2007).
[17] T. Damour, A. Nagar, E. N. Dorband, D. Pollney, and L. Rezzolla, Phys. Rev. D **77**, 084017 (2008).
[18] A. Nagar, P. Rettegno, R. Gamba, S. Albanesi, A. Albertini, and S. Bernuzzi, Phys. Rev. D **108**, 124018 (2023).
[19] L. Pompili *et al.*, Phys. Rev. D **108**, 124035 (2023).
[20] T. Damour and A. Nagar, Phys. Rev. D **81**, 084016 (2010).
[21] T. Damour, A. Nagar, and L. Villain, Phys. Rev. D **85**, 123007 (2012).
[22] A. Nagar *et al.*, Phys. Rev. D **98**, 104052 (2018).
[23] T. Dietrich *et al.*, Phys. Rev. D **99**, 024029 (2019).
[24] D. Chiaramello and A. Nagar, Phys. Rev. D **101**, 101501 (2020).
[25] A. Nagar, P. Rettegno, R. Gamba, and S. Bernuzzi, Phys. Rev. D **103**, 064013 (2021).
[26] A. Nagar, A. Bonino, and P. Rettegno, Phys. Rev. D **103**, 104021 (2021).
[27] M. Khalil, A. Buonanno, J. Steinhoff, and J. Vines, Phys. Rev. D **104**, 024046 (2021).
[28] A. Placidi, S. Albanesi, A. Nagar, M. Orselli, S. Bernuzzi, and G. Grignani, Phys. Rev. D **105**, 104030 (2022).
[29] A. Ramos-Buades, A. Buonanno, M. Khalil, and S. Ossokine, Phys. Rev. D **105**, 044035 (2022).
[30] S. Albanesi, A. Placidi, A. Nagar, M. Orselli, and S. Bernuzzi, Phys. Rev. D **105**, L121503 (2022).
[31] A. Nagar, R. Gamba, P. Rettegno, V. Fantini, and S. Bernuzzi, Phys. Rev. D **110**, 084001 (2024).
[32] A. Nagar, D. Chiaramello, R. Gamba, S. Albanesi, S. Bernuzzi, V. Fantini, M. Panzeri, and P. Rettegno, Phys. Rev. D **111**, 064050 (2025).
[33] A. Buonanno, Y. Chen, and T. Damour, Phys. Rev. D **74**, 104005 (2006).
[34] Y. Pan, A. Buonanno, A. Taracchini, L. E. Kidder, A. H. Mroue, H. P. Pfeiffer, M. A. Scheel, and B. Szilágyi, Phys. Rev. D **89**, 084006 (2014).
[35] S. Akcay, R. Gamba, and S. Bernuzzi, Phys. Rev. D **103**, 024014 (2021).

[36] R. Gamba, S. Akçay, S. Bernuzzi, and J. Williams, Phys. Rev. D **106**, 024020 (2022).
[37] M. Khalil, A. Buonanno, H. Estelles, D. P. Mihaylov, S. Ossokine, L. Pompili, and A. Ramos-Buades, Phys. Rev. D **108**, 124036 (2023).
[38] A. Ramos-Buades, A. Buonanno, H. Estellés, M. Khalil, D. P. Mihaylov, S. Ossokine, L. Pompili, and M. Shiferaw, Phys. Rev. D **108**, 124037 (2023).
[39] A. Gonzalez, R. Gamba, M. Breschi, F. Zappa, G. Carullo, S. Bernuzzi, and A. Nagar, Phys. Rev. D **107**, 084026 (2023).
[40] R. Gamba and S. Bernuzzi, Phys. Rev. D **107**, 044014 (2023).
[41] R. Gamba *et al.*, arXiv:2307.15125.
[42] R. Gamba, D. Chiaramello, and S. Neogi, Phys. Rev. D **110**, 024031 (2024).
[43] T. Regge and J. A. Wheeler, Phys. Rev. **108**, 1063 (1957).
[44] F. J. Zerilli, Phys. Rev. Lett. **24**, 737 (1970).
[45] A. Nagar and L. Rezzolla, Classical Quantum Gravity **22**, R167 (2005).
[46] K. Martel and E. Poisson, Phys. Rev. D **71**, 104003 (2005).
[47] S. A. Teukolsky, Astrophys. J. **185**, 635 (1973).
[48] S. Bernuzzi and A. Nagar, Phys. Rev. D **81**, 084056 (2010).
[49] S. Bernuzzi, A. Nagar, and A. Zenginoglu, Phys. Rev. D **84**, 084026 (2011).
[50] S. Bernuzzi, A. Nagar, and A. Zenginoglu, Phys. Rev. D **86**, 104038 (2012).
[51] E. Harms, S. Bernuzzi, A. Nagar, and A. Zenginoglu, Classical Quantum Gravity **31**, 245004 (2014).
[52] V. Varma, S. E. Field, M. A. Scheel, J. Blackman, L. E. Kidder, and H. P. Pfeiffer, Phys. Rev. D **99**, 064045 (2019).
[53] T. Chu, H. P. Pfeiffer, and M. A. Scheel, Phys. Rev. D **80**, 124051 (2009).
[54] G. Lovelace, M. Scheel, and B. Szilagyi, Phys. Rev. D **83**, 024010 (2011).
[55] G. Lovelace, M. Boyle, M. A. Scheel, and B. Szilagyi, Classical Quantum Gravity **29**, 045003 (2012).
[56] L. T. Buchman, H. P. Pfeiffer, M. A. Scheel, and B. Szilagyi, Phys. Rev. D **86**, 084033 (2012).
[57] D. A. Hemberger, G. Lovelace, T. J. Loredo, L. E. Kidder, M. A. Scheel, B. Szilágyi, N. W. Taylor, and S. A. Teukolsky, Phys. Rev. D **88**, 064014 (2013).
[58] M. A. Scheel, M. Giesler, D. A. Hemberger, G. Lovelace, K. Kuper, M. Boyle, B. Szilágyi, and L. E. Kidder, Classical Quantum Gravity **32**, 105009 (2015).
[59] J. Blackman, S. E. Field, C. R. Galley, B. Szilágyi, M. A. Scheel, M. Tiglio, and D. A. Hemberger, Phys. Rev. Lett. **115**, 121102 (2015).
[60] G. Lovelace *et al.*, Classical Quantum Gravity **32**, 065007 (2015).
[61] A. H. Mroue, M. A. Scheel, B. Szilagyi, H. P. Pfeiffer, M. Boyle *et al.*, Phys. Rev. Lett. **111**, 241104 (2013).
[62] P. Kumar, K. Barkett, S. Bhagwat, N. Afshari, D. A. Brown, G. Lovelace, M. A. Scheel, and B. Szilágyi, Phys. Rev. D **92**, 102001 (2015).
[63] T. Chu, H. Fong, P. Kumar, H. P. Pfeiffer, M. Boyle, D. A. Hemberger, L. E. Kidder, M. A. Scheel, and B. Szilagyi, Classical Quantum Gravity **33**, 165001 (2016).
[64] M. Boyle *et al.*, Classical Quantum Gravity **36**, 195006 (2019).
[65] SXS Gravitational Waveform Database, https://data.black-holes.org/waveforms/index.html.
[66] K. Mitman *et al.*, Phys. Rev. D **104**, 024051 (2021).
[67] T. Damour and A. Nagar, Phys. Rev. D **90**, 024054 (2014).
[68] D. Hilbert, *Grundzüge einer allgemeinen Theorie der linearen Integralgleichungen* (B.G. Teubner, Leipzig, 1912).
[69] R. N. Bracewell, *The Fourier Transform and Its Applications* (McGraw-Hill, New York, 2000).
[70] D. Christodoulou, Phys. Rev. Lett. **67**, 1486 (1991).
[71] K. S. Thorne, Phys. Rev. D **45**, 520 (1992).
[72] L. Blanchet and T. Damour, Phys. Rev. D **46**, 4304 (1992).
[73] K. Mitman *et al.*, Classical Quantum Gravity **41**, 223001 (2024).
[74] M. Favata, Phys. Rev. D **80**, 024002 (2009).
[75] K. Cunningham, C. Kavanagh, A. Pound, D. Trestini, N. Warburton, and J. Neef, arXiv:2410.23950.
[76] M. Favata, Astrophys. J. Lett. **696**, L159 (2009).
[77] M. Favata, Classical Quantum Gravity **27**, 084036 (2010).
[78] M. Favata, Phys. Rev. D **84**, 124013 (2011).
[79] M. Ebersold, Y. Boetzel, G. Faye, C. K. Mishra, B. R. Iyer, and P. Jetzer, Phys. Rev. D **100**, 084043 (2019).
[80] E. Grilli, A. Placidi, S. Albanesi, G. Grignani, and M. Orselli, Phys. Rev. D **111**, 044045 (2025).
[81] D. Pollney and C. Reisswig, Astrophys. J. Lett. **732**, L13 (2011).
[82] K. Mitman, J. Moxon, M. A. Scheel, S. A. Teukolsky, M. Boyle, N. Deppe, L. E. Kidder, and W. Throwe, Phys. Rev. D **102**, 104007 (2020).
[83] N. T. Bishop, R. Gomez, L. Lehner, and J. Winicour, Phys. Rev. D **54**, 6153 (1996).
[84] C. Reisswig, N. T. Bishop, D. Pollney, and B. Szilagyi, Classical Quantum Gravity **27**, 075014 (2010).
[85] J. Moxon, M. A. Scheel, and S. A. Teukolsky, Phys. Rev. D **102**, 044052 (2020).
[86] J. Moxon, M. A. Scheel, S. A. Teukolsky, N. Deppe, N. Fischer, F. Hébert, L. E. Kidder, and W. Throwe, Phys. Rev. D **107**, 064013 (2023).
[87] N. Deppe *et al.*, Spectre (2024), 10.5281/zenodo.10967177.
[88] H. Bondi, M. G. J. van der Burg, and A. W. K. Metzner, Proc. R. Soc. A **269**, 21 (1962).
[89] R. K. Sachs, Proc. R. Soc. A **270**, 103 (1962).
[90] C. Talbot, E. Thrane, P. D. Lasky, and F. Lin, Phys. Rev. D **98**, 064031 (2018).
[91] K. Mitman *et al.*, Phys. Rev. D **103**, 024031 (2021).
[92] Z. Cao and W.-B. Han, Classical Quantum Gravity **33**, 155011 (2016).
[93] M. Rosselló-Sastre, S. Husa, and S. Bera, Phys. Rev. D **110**, 084074 (2024).
[94] O. M. Boersma, D. A. Nichols, and P. Schmidt, Phys. Rev. D **101**, 083026 (2020).
[95] M. Hübner, C. Talbot, P. D. Lasky, and E. Thrane, Phys. Rev. D **101**, 023011 (2020).
[96] A. M. Grant and D. A. Nichols, Phys. Rev. D **107**, 064056 (2023); **108**, 029901(E) (2023).
[97] B. Goncharov, L. Donnay, and J. Harms, Phys. Rev. Lett. **132**, 241401 (2024).
[98] S. Gasparotto, R. Vicente, D. Blas, A. C. Jenkins, and E. Barausse, Phys. Rev. D **107**, 124033 (2023).

[99] H. Inchauspé, S. Gasparotto, D. Blas, L. Heisenberg, J. Zosso, and S. Tiwari, Phys. Rev. D **111**, 044044 (2025).
[100] Y. Xu, M. Rosselló-Sastre, S. Tiwari, M. Ebersold, E. Z. Hamilton, C. García-Quirós, H. Estellés, and S. Husa, Phys. Rev. D **109**, 123034 (2024).
[101] J. Yoo *et al.*, Phys. Rev. D **108**, 064027 (2023).
[102] K. Mitman *et al.*, Phys. Rev. D **106**, 084029 (2022).
[103] A. Pound, Fund. Theor. Phys. **179**, 399 (2015).
[104] S. Bernuzzi, A. Nagar, and A. Zenginoglu, Phys. Rev. D **83**, 064010 (2011).
[105] A. Taracchini, A. Buonanno, G. Khanna, and S. A. Hughes, Phys. Rev. D **90**, 084025 (2014).
[106] S. Albanesi, S. Bernuzzi, T. Damour, A. Nagar, and A. Placidi, Phys. Rev. D **108**, 084037 (2023).
[107] See Supplemental Material at http://link.aps.org/supplemental/10.1103/PhysRevD.111.L121501 for technical details on post-merger fits and next-to-quasi-circular corrections, which includes Refs. [108–119].
[108] C. J. Woodford, M. Boyle, and H. P. Pfeiffer, Phys. Rev. D **100**, 124010 (2019).
[109] J. Healy, C. O. Lousto, Y. Zlochower, and M. Campanelli, Classical Quantum Gravity **34**, 224001 (2017).
[110] J. Healy, C. O. Lousto, J. Lange, R. O'Shaughnessy, Y. Zlochower, and M. Campanelli, Phys. Rev. D **100**, 024021 (2019).
[111] J. Healy and C. O. Lousto, Phys. Rev. D **102**, 104018 (2019).
[112] J. Healy and C. O. Lousto, Phys. Rev. D **105**, 124010 (2022).
[113] S. Albanesi, A. Nagar, and S. Bernuzzi, Phys. Rev. D **104**, 024067 (2021).
[114] T. Damour, B. R. Iyer, and A. Nagar, Phys. Rev. D **79**, 064004 (2009).
[115] T. Damour and A. Nagar, Phys. Rev. D **90**, 044018 (2014).
[116] C. M. Biwer, C. D. Capano, S. De, M. Cabero, D. A. Brown, A. H. Nitz, and V. Raymond, Publ. Astron. Soc. Pac. **131**, 024503 (2019).
[117] Y. Chen *et al.*, Phys. Rev. D **110**, 064049 (2024).
[118] J. Valencia, R. Tenorio, M. Rosselló-Sastre, and S. Husa, Phys. Rev. D **110**, 124026 (2024).
[119] I. Harry, J. C. Bustillo, and A. Nitz, Phys. Rev. D **97**, 023004 (2018).
[120] A. Ori and K. S. Thorne, Phys. Rev. D **62**, 124022 (2000).
[121] R. H. Price, Phys. Rev. D **5**, 2419 (1972).
[122] E. W. Leaver, Phys. Rev. D **34**, 384 (1986).
[123] N. Andersson, Phys. Rev. D **55**, 468 (1997).
[124] M. De Amicis, S. Albanesi, and G. Carullo, Phys. Rev. D **110**, 104005 (2024).
[125] M. De Amicis *et al.*, arXiv:2412.06887.
[126] S. Ma, M. A. Scheel, J. Moxon, K. C. Nelli, N. Deppe, L. E. Kidder, W. Throwe, and N. L. Vu, arXiv:2412.06906.
[127] V. Cardoso, G. Carullo, M. De Amicis, F. Duque, T. Katagiri, D. Pereniguez, J. Redondo-Yuste, T. F. M. Spieksma, and Z. Zhong, Phys. Rev. D **109**, L121502 (2024).
[128] T. Islam, G. Faggioli, G. Khanna, S. E. Field, M. van de Meent, and A. Buonanno, arXiv:2407.04682.
[129] J. G. Baker, W. D. Boggs, J. Centrella, B. J. Kelly, S. T. McWilliams, and J. R. van Meter, Phys. Rev. D **78**, 044046 (2008).
[130] R. Cotesta, A. Buonanno, A. Bohé, A. Taracchini, I. Hinder, and S. Ossokine, Phys. Rev. D **98**, 084028 (2018).
[131] X. Jiménez-Forteza, D. Keitel, S. Husa, M. Hannam, S. Khan, and M. Pürrer, Phys. Rev. D **95**, 064024 (2017).
[132] A. Nagar, G. Riemenschneider, G. Pratten, P. Rettegno, and F. Messina, Phys. Rev. D **102**, 024077 (2020).
[133] A. Placidi, G. Grignani, T. Harmark, M. Orselli, S. Gliorio, and A. Nagar, Phys. Rev. D **108**, 024068 (2023).
[134] Updated Advanced LIGO sensitivity design curve, https://dcc.ligo.org/LIGO-T1800044/public.
[135] M. Boyle, Phys. Rev. D **87**, 104006 (2013).
[136] M. Boyle, L. E. Kidder, S. Ossokine, and H. P. Pfeiffer, arXiv:1409.4431.
[137] M. Boyle, Phys. Rev. D **93**, 084031 (2016).
[138] M. Boyle, D. Iozzo, and L. C. Stein, moble/SCRI: v1.2 (2020), 10.5281/zenodo.4041972.
[139] https://bitbucket.org/teobresums/teobresums/src/
[140] F. Crameri, Scientific colour maps (2023), 10.5281/zenodo.8409685.